Vol. 47, No. 3 (2025) 567-582, DOI: 10.24874/ti.1907.02.25.05

Tribology in Industry

www.tribology.rs

RESEARCH

Multi Criteria Optimization of Al/Al_2O_3 Functionally Graded Composite Fabricated Using Grey Relational Analysis

Aravind Tripathy[a], Pragyan Senapati[a,*], Saroj Kumar Sarangi[b], Anil Kumar Chaubey[c]

[a]*ITER, SOA University, ITER College Rd, Jagmohan Nagar, Bhubaneswar, Odisha 751030, India,*
[b]*NIT Jamshedpur, Adityapur, Jamshedpur, Jharkhand-831014, India,*
[c]*CSIR-IMMT, Bhubaneswar, Odisha-751013, India.*

Keywords:

FGCM
PM
GRA
COF
Wear rate
Specific wear rate
Relative wear resistance

* Corresponding author:

Pragyan Senapati
Email: pragyansenapati@soa.ac.in

Received: 22 February 2025
Revised: 6 April 2025
Accepted: 24 May 2025

A B S T R A C T

A six-layered Al/Al_2O_3 functionally graded composite material (FGCM) was successfully fabricated via powder metallurgy (PM), with each layer approximately 1.5 mm. thick. The influence of varying Al_2O_3 volume fractions on the microstructure, hardness and tribological properties (wear rate, specific wear rate, relative wear resistance and coefficient of friction) was systematically evaluated. Grey Relational Analysis (GRA)was effectively utilized for multi-criteria optimization, revealing that, relative wear resistance significantly influences the wear stability of the FGCM. Optimal performance was achieved at an intermediate Al/ Al_2O_3 fraction (e.g., 30%), resulting in notably enhanced wear resistance. The study demonstrates the efficacy of integrating PM fabrication and GRA optimization in producing FGCMs suitable for demanding applications in automotive and aerospace industries.

1. INTRODUCTION

Functionally Graded Composite Materials (FGCM) represents a cutting-edge class of composite materials, engineered to exhibit continuous and gradual variations in composition, structure, and properties [1]. Upon knowingly designing gradients in specific directions or orientations, FGCM outperforms homogeneous materials composed of similar constituents, offering enhanced performance and functionality [2-4]. FGCM exhibits continuous and smooth variations in mechanical properties, including Young's modulus, Poisson's ratio, shear modulus, and density, in preferred directions [5-6]. Researchers have developed functionally graded materials to address the increasing

demand for materials that offer multiple functionalities and can perform well in challenging environments, such as those found in aerospace applications [7]. The outstanding stiffness-to-weight ratio of functionally graded materials has contributed to their widespread adoption. Current research priorities include developing efficient, cost-effective methods for bulk production [8-9]. Among most popular assembly procedures like powder metallurgy (PM), solid freeform fabrication, laser cladding, selective laser sintering, 3-D printing and selective laser melting etc. one may opt for a process depending on various factors (i.e. material compatibility, desired property gradient, part geometry and complexity, production volume, processing capabilities, post-processing requirements, environmental impact) the most prominent among them being the cost factor [10-12]. Alumina (Al_2O_3) is a commonly used ceramic reinforcement in functionally graded composites due to its exceptional hardness, wear resistance, and thermal stability [13]. The addition of alumina particles to the aluminium matrix has been found to dramatically enhance the hardness and sliding wear resistance of these composites [14-16]. The hard alumina particles act as load-bearing components, effectively increasing the overall hardness and wear resistance of the functionally graded material [17-18]. The gradual increase in alumina content from the metal-rich to the ceramic-rich regions of the composite provides a smooth transition in mechanical properties, contributing to its improved tribological performance [19-20]. Furthermore, the interface between the Aluminium and Alumina in the functionally graded composite plays a crucial role in determining the wear characteristics. A strong interfacial bond between the matrix and the reinforcement ensures efficient load transfer, preventing the pullout or fracture of the hard ceramic particles during wear [21-22].

Applications of FGCM: These engineered materials have found multiple fronts of application, right from aerospace to modern electronics (computer hardware and robotics etc.), with the aim of optimizing the use of available materials' inherent properties. These materials are used in a range of applications, including aerospace engineering (aircraft and spacecraft), biomedical devices (implants), industrial equipment (heat exchangers, engine components), and energy applications (fusion reactors). Metal-ceramic composites are among the most common FGMs, where the ceramic portion offer excellent thermal barrier characteristics while the metallic portions offer superior fracture toughness property [23-24]. Shown below (Fig. 1) the schematic of the metal-ceramic FGM microstructure.

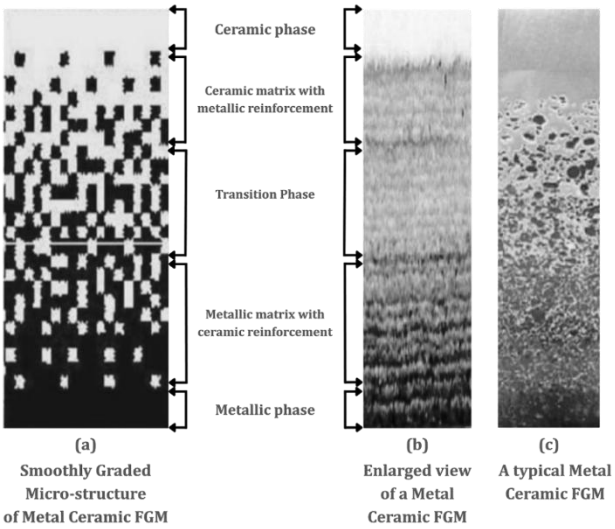

Fig. 1. Schematics of Metal-Ceramic FGM microstructure.

These engineered materials (FGMs) commonly involve two phases of isotropic materials, although many material configurations are possible; typical components include metal alloys like magnesium, Aluminium, Copper, Titanium, Tungsten, and Steel and advanced ceramics such as Zirconia, Alumina, Silicon Carbide, and Tungsten Carbide.

In summary, the incorporation of hard and wear-resistant alumina particles into the aluminum matrix, along with the functionally graded structure, significantly enhances the hardness and wear resistance of these composites. Here through this endeavor, the authors have tried to address the parametric process effect on the fabrication of Al-Alumina FGCM using uniaxial hot press following the powder metallurgy route (particle size, mixing the different constituents, volume fraction of reinforcement (Alumina) in the mixture, and pressing parameters playing the key role).

Thus Al-Al_2O_3 FGCM samples were fabricated using the PM route as illustrated in Fig. 2 below.

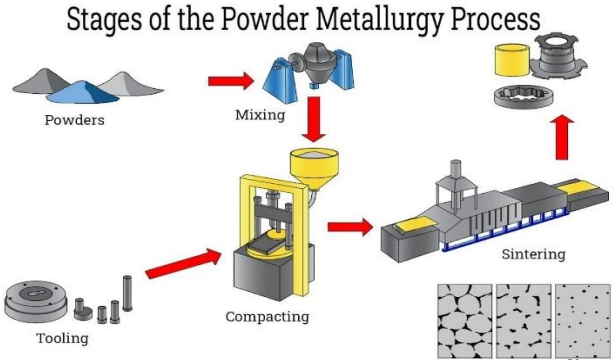

Fig. 2. Schematic view of powder metallurgy process with hot press used for sample fabrication.

To investigate the tribological performance of these composites, key process parameters such as speed, load, time, and percentage of Al_2O_3 reinforcement based on their influence on wear characteristics, has been selected as identified in prior studies [25-27]. These parameters were systematically varied to optimize wear rate, specific wear rate, relative wear_resistance, and coefficient of friction (COF), with the goal of identifying optimal conditions for enhanced tribological performance.

To efficiently explore the effects and interactions of these parameters, the Taguchi's L_{16} orthogonal array design with spindle speed (300, 350, 400, 450 RPM), load (30, 35, 40, 45 N), and fixed levels of time (30 minutes) and Al_2O_3 reinforcement (30%) has been employed (Table 1).

Table 1. Process parameters at different levels.

Level	Sample Sintering Temp (^{0}C)	Speed	Load	Relative Sliding Speed
1	400	300 350 400 450	30 35 40 45	0.52m/s
2	450	300 350 400 450	30 35 40 45	0.52m/s

Taguchi's L_{16} orthogonal array design has been utilized considering the various point boundaries combined with the above-stated parameters, which has not been referred to earlier in the past works [28]. Unlike previous studies [28], which did not apply this design to the specific combination of parameters and boundary conditions for Al-Al_2O_3 FGCM, our approach ensures a robust and systematic evaluation of tribological properties.

The Grey relation analysis (GRA) approach has been adopted in the present work in proceeding fabrication parameters of Al-Al_2O_3 FGCMs. Thus, by applying Taguchi's L_{16} plan of design [26-27], it is to confirm the engineered material has achieved the desired quality and reliability through the established process route, which can be universally accepted for greater challenges in the field of science and technology.

2. MATERIALS AND METHODS

From available research papers it is clearly understood that for the various advantages of Al-Al_2O_3 functionally graded composite materials, it has a great demand as well as future prospects among the advanced engineered materials, which is still evolving. As an important material for engineering applications, wear characteristics plays a very vital role in defining the overall life and stability of the component or assembly, and the wear property can be tailored as per requirement by altering the composition, position, and other relevant process parameters.

The Al-Al_2O_3 samples, which were fabricated using a uniaxial hot press and sintered at 400^{0}C and 450^{0}C respectively were subjected to a wear resistance test in the ceramic (Al_2O_3)-rich surface for a thirty-minute cycle on a Ducom's TR-20 model pin on disc wear measurement device maintained at room temperature and with rpm 300, a comparative sliding speed of 0.52m/s and at three distinct loads of 30, 35 and 40 Newtons correspondingly.

In this present work, before conducting the experiments, many trials were conducted with varying sintering temperatures to find the best sintering temperature for such FGCM for low weight and superior strength application. It was followed by wear tests which were carried out with varying speeds, and loads for the best possible results. After studying the results, an appropriate set of parameters was selected to restrict wear characteristic of the Al-Al_2O_3 functionally graded composite material and also zeroed in on the best temperature at which the component is to be fabricated in

order to develop the required material properties that would eventually restrict wear to the optimum level. With each experimental set up, four sets of trials were carried out. For detailed analysis the average value of the above trials was considered. For each set of trials, a new tool was used so that the tool wear condition was as minimal as possible.

2.1 Experimental procedure of wear test

Ducom's pin-on-disc machine, (Fig. 3) Model: TR-20, Wear & Friction Monitor was used for the dry sliding wear tests for different number of specimens as per ASTM G99 [29].

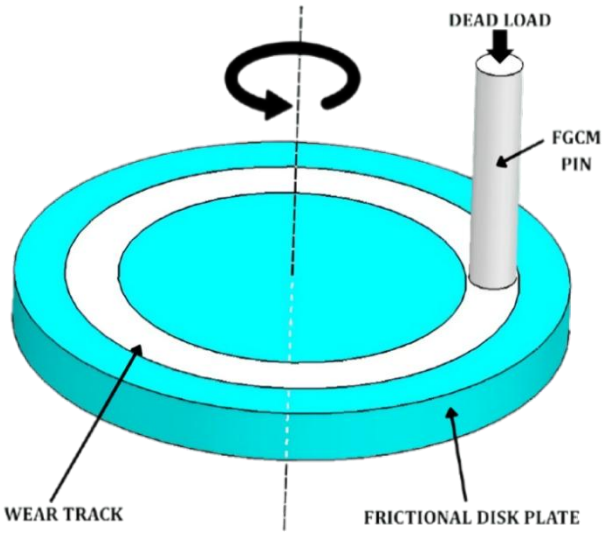

Fig. 3. Schematic view of the pin-on-disk machine set up.

A notable feature of this machine is its interchangeable setup, allowing for a quick transformation from a rotary tribometer to a linear reciprocating tribometer in less than two minutes. Precise motion control and customizable movement options provide added flexibility. This machine boasts an innovative design, enabling effortless conversion between rotary and linear reciprocating tribometer configurations within minutes. Advanced motion control and versatile movement options further enhance experimental capabilities. Wear characteristics are determined by the following calculation:

Area (A) = πr^2

Volume loss = Area × height loss

Wear rate = volume loss / distance slid

Wear resistance $\propto$ 1/ wear rate

Specific wear rate=wear rate / load

2.2 Design of experiments

By studying various available literatures and with the reference to the outcomes of the trials in this specific area, the independent process parameters were identified and using Minitab software, an experiment was designed by applying fundamentals of the Taguchi L_{16} design of experiment [29]. The process variables with its limits were tabulated below in Table 2. The process parameters at 400^{0}C and 450^{0}C sample sintering temperature are given in Table 3 and Table 4 respectively.

Table 2. Process variables and its limits.

Variation of Variable	Sintering Temperature (^{0}C)	Spindle speed (RPM)	Load (N)
1	400	300	30
2	450	350	35
3	-	400	40
4	-	450	45

Table 3. Process parameters at sintering temperature of 400^{0}C.

Factors	Parameters	Level-1			
A	Sintering temperature (^{0}C)	400	400	400	400
B	Spindle speed (RPM)	300	350	400	450
C	Load(N)	30	35	40	45

Table 4. Process parameters at sintering temperature of 450^{0}C.

Factors	Parameters	Level-1			
A	Sintering temperature(^{0}C)	450	450	450	450
B	Spindle speed (RPM)	300	350	400	450
C	Load(N)	30	35	40	45

2.3 Optimization technique using Grey relational analysis (GRA)

GRA stands out as a user-friendly optimization technique, ideal for addressing problems with incomplete, ambiguous, or undefined data, as well as multiple inputs. The GRA follows various equations as depicted below (Eq1-9). The "grey" concept bridges the gap between unclear ("black") and clear ("white") information. The optimization process using the GRA technique follows the following steps:

2.3.1 Data pre-processing / data normalization

In the pre-processing phase, the "smaller the better" approach was (Eq.2) adopted for normalizing the experimental data and enumerated below, and the values lie between zero (insignificant information) and one (significant information).

2.3.2 Tabulation of grey relational coefficient

For each of the normalized values obtained a grey relational coefficient was found by using (Eq. 5) as described below.

2.3.3 Tabulation of grey relational grade

By taking the average of all grey relational coefficients (Eq. 9), the grey relational grade was obtained.

2.3.4 Optimal process parameter assessment

Optimal process parameters were calculated using Taguchi analysis of variance.

2.4 Data normalization / data pre-processing

Data normalization reduces inconsistencies in the data, accounting for varying ranges and units among performance characteristics. This step is crucial in data preprocessing. Normalization methods depend on the original sequence's set point value. Normalization is applied to reduce data inconsistencies, addressing differences in range and units. This initial data pre-processing step extracts analogous series from the original experimental data. Depending on the set point value, three normalization approaches exist. For sequences with infinite set points, a 'larger-the-better' characteristic is applied (Eq. 1).

$$x_i^*(k) = \frac{x_i^0(k) - \min x_i^0(k)}{max x_i^0(k) - \min x_i^0(k)} \quad (1)$$

Nevertheless, using the 'smaller the better' principle, the original sequence could be normalized as follows (Eq. 2):

$$x_i^*(k) = \frac{\max x_i^0(k) - x_i^0(k)}{max x_i^0(k) - \min x_i^0(k)} \quad (2)$$

The original sequence can be normalized if it has a definite set point value with following (Eq. 3):

$$x_i^*(k) = 1 - \frac{|x_i^*(k) - x^0|}{max x_i^0(k) - x^0} \quad (3)$$

However, normalization can be achieved through simple agreement and the greatest elementary process of standardization, presented as follows (Eq. 4):

$$x_i^*(k) = \frac{x_i^0(k)}{x_i^0(1)} \quad (4)$$

In the above equation, $x_i^0(k)$ denotes the original sequence of the performance characteristic, $x_i^*(k)$, pointing out the normalized sequence max $x_i^*(k)$ is the maximum magnitude of $x_i^0(k)$ and the least $x_i^*(k)$ being the minimum magnitude of $x_i^0(k)$ and x^0 are the recent preferred magnitudes.

2.5 Grey relational analysis coefficient and grade evaluation

The Grey Relational Analysis procedure begins with determining the Grey Relational Coefficient based on the normalized database. Then, with the help of this Grey Relational Coefficient, a Grey Relational Grade is established. By this process, we not only measure the relevancy of the two systems but also establish a relationship between them. Thus, the method of calculating the grey relational coefficient ξ(k) is established as follows (Eq. 5):

$$\xi(k) = \frac{\Delta_{min} + \xi \Delta_{max}}{\Delta_{0i}(k) + \xi \Delta_{max}} \quad (5)$$

In Eq. (6), the difference between the original sequence $x_i^0(k)$ and the sequence after normalization $x_i^*(k)$ is denoted by Δ_{0i}, this concept is also termed as the deviation sequence, with 'ξ' being the distinguishing coefficient. It's worth noting that a smaller ξ value is associated with higher distinguishing significance. The formula for minimum and maximum deviation sequence is given in Eq. 7 and Eq. 8 respectively. In general, ξ = 0.5 is usually considered.

$$\Delta_{0i} = \left\| x_0^*(k) - x_i^0(k) \right\| \quad (6)$$

$$\Delta_{min} = \frac{min}{\forall j \in i} \frac{min}{\forall k} \left\| x_0^*(k) - x_j^*(k) \right\| \quad (7)$$

$$\Delta_{max} = \frac{max}{\forall j \in i} \frac{max}{\forall k} \left\| x_0^*(k) - x_j^*(k) \right\| \quad (8)$$

The grey relational grade is calculated by taking the average of the grey relational coefficients derived earlier, utilizing the Eq. 9 shown below:

$$\gamma i = \frac{1}{n}\sum_{k=1}^{n} \xi_i(k) \quad (9)$$

The schematic flow process chart for this experiment is given below in Fig. 4.

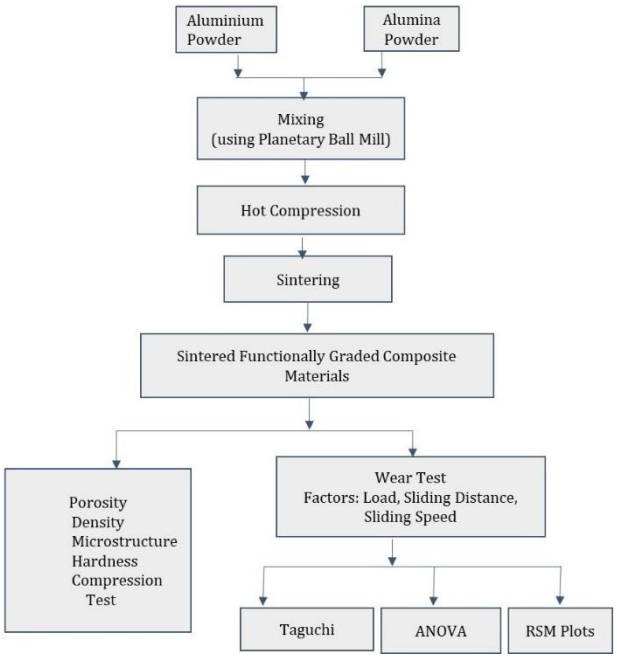

Fig. 4. Schematic view of the Methodology used.

3. A BRIEF DESCRIPTION ABOUT APPARATUS USED

3.1 Hardness tester

A device used to measure the hardness of the fabricated Al/Al_2O_3 composite materials. The hardness tester will help evaluate the mechanical properties of the composite, which is crucial for experiencing its potential applications.

3.2 Test specimens

Samples of the fabricated Al/Al_2O_3 composite materials prepared for various tests, such as hardness, tensile strength, and microstructural analysis. These specimens will be used to evaluate the properties of the composite and validate the effectiveness of the GRA technique.

3.3 Microscope

An optical or electron microscope used to examine the microstructure of the fabricated Al/ Al_2O_3 composite materials. The microscope will help analyze the distribution of Al_2O_3 particles, porosity, and other microstructural features that affect the properties of the composite.

3.4 Calibration standards

Reference materials or standards used to calibrate the hardness tester, microscope, and other equipment used in the fabrication and testing of the Al/ Al_2O_3 composite materials. Calibration standards ensure the accuracy and reliability of the test results, which is crucial for validating the GRA technique.

3.5 Scanning electron microscope (SEM)

A high-resolution imaging tool used to examine the microstructure and morphology of the fabricated Al/ Al_2O_3 composite materials. The SEM will help analyze the distribution of Al_2O_3 particles, porosity, and other microstructural features that affect the properties of the composite.

3.6 Sample preparation equipment

Machines and tools used to prepare the Al/ Al_2O_3 composite samples for SEM analysis, such as cutting, polishing, and coating. Proper sample preparation is crucial for obtaining high-quality SEM images and accurate microstructural analysis.

3.7 Detector

A device used in conjunction with the SEM to detect and analyze the signals generated by the interaction between the electron beam and the sample. The detector will help gather information on the composition, crystal structure, and other properties of the Al/ Al_2O_3 composite materials.

3.8 Safety equipment

Protective gear and devices used to ensure the safety of personnel involved in the fabrication of Al/ Al_2O_3 composite materials using the GRA technique. This includes gloves, goggles, face masks, and other personal protective equipment (PPE) to prevent injury from chemicals, particles, and equipment.

3.9 Power supply

A device that provides the necessary electrical power to operate uni-axial hot compression mold, the equipment used in the PM process to fabricate the FGCM by using the established GRA technique. A stable and reliable power supply is crucial for maintaining consistent processing conditions and ensuring the quality of the fabricated composite materials.

4. RESULTS AND DISCUSSIONS

4.1 Microstructure and hardness

Observations from Fig. 5 (a), (b) and (c) and Fig. 6 reveal that the joined material exhibits a layered microstructure, characterized by an Al matrix phase and uniformly distributed Al_2O_3 phases.

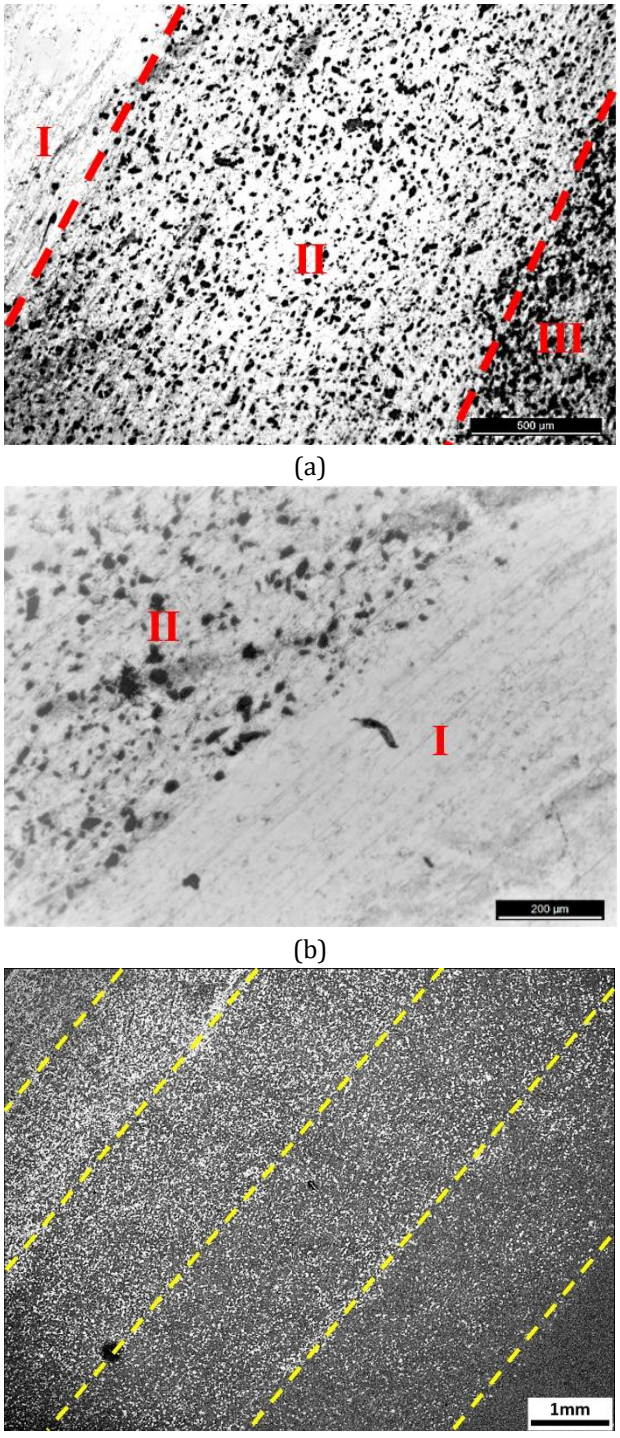

Fig. 5. (a), (b) Optical images of the Al/Al_2O_3 FGM microstructure, (c) FESEM image of Al/Al_2O_3 FGM-depicting microstructural analysis.

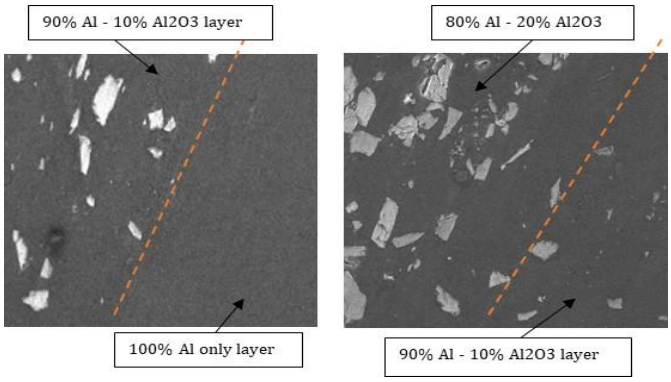

Fig. 6. FESEM image of Al/ Al_2O_3 FG sample showing layers with different compositions.

Figure 7 illustrates the hardness variation across different layers of the FGM sample, revealing a significant increase in hardness due to the presence of Al_2O_3 particulate reinforcement. The hardness rises from 35.2 HV in the 100% Aluminum layer to 74.8 HV in the 50% Al and 50% Al_2O_3 layer. The micro-hardness of the FGM sample increases steadily from 35.2 HV to 74.8 HV across the layers, with a notable 33% rise in the second layer containing 10% Al_2O_3. This trend indicates strong interfacial bonding between the Aluminum matrix and Alumina particles. As shown in Figure 6, the hardness of the FGM sample varies significantly across the layers, with a substantial increase attributed to the addition of Al_2O_3 particulate reinforcement. The hardness increases by 33% in the second layer and continues to rise steadily, indicating enhanced interfacial bonding.

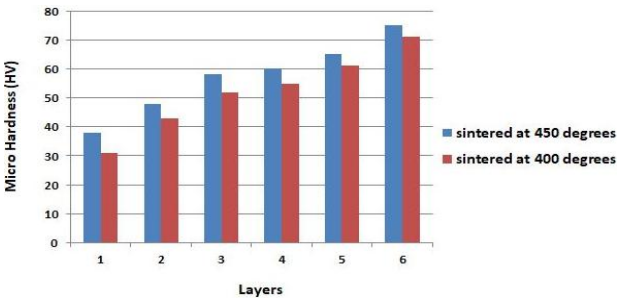

Fig. 7. Micro hardness values of the FGM sample at individual layers.

4.2. Analysis of wear rate

The fabricated samples were sintered at 400^{0}C and 450^{0}C respectively. Dry sliding wear behavior of the composite were studied [30]. The wear resistance of the samples was evaluated using Ducom's (Model-RT-20) pin-on-disc wear tester. The test parameters included a 30-minute duration, 300 rpm, 0.52 m/s sliding speed, and loads of 30, 35, and 40 N at ambient temperature.

For the above mentioned, fabricated samples, the rate of wear increases, while resistance to wear decreases with an increase in load (Tables 5 & 6).

Table 5. Wear test data for sample sintered at 400 ^{0}C.

Load (N)	COF (μ)	Wear Rate (mm^3/m)	Specific Wear Rate (mm^3/N-m)	Wear Resistance
30	0.077	0.1204	0.0041	8.3132
35	0.067	0.1234	0.0035	8.1053
40	0.059	0.1265	0.0032	7.9076

Table 6. Wear test data for sample sintered at 450 ^{0}C.

Load (N)	COF (μ)	Wear Rate (mm^3/m)	Specific Wear Rate (mm^3/N-m)	Wear Resistance
30	0.0774	0.1235	0.0042	8.1054
35	0.0677	0.1295	0.0037	7.7193
40	0.0605	0.1357	0.0034	7.3684

In Fig. 8, the variation of wear rate with respect to COF and load has been plotted. Fig. 9 and Fig. 10 depict the surface plot (wireframe) and contour plot of wear rate with respect to COF and load for the sample sintered at 400^{0}C respectively.

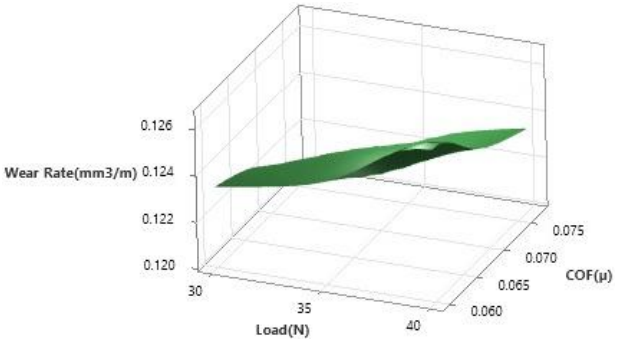

Fig. 8. Surface Plot of Wear Rate vs COF and Load for the sample sintered at 400^{0}C.

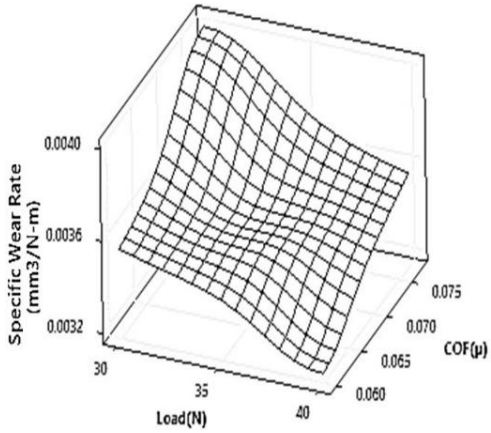

Fig. 9. Surface Plot (Wire-frame) of Specific Wear Rate (mm^3/m) vs CoF and Load for the sample sintered at 400^{0}C.

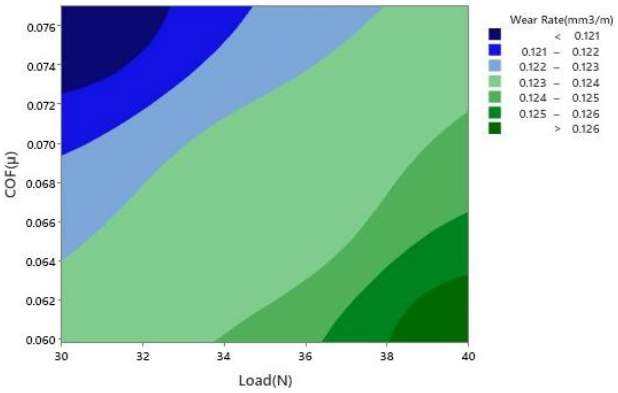

Fig. 10. Contour Plot of Wear Rate vs COF and Load for the sample sintered at 400^{0}C

For the fabricated samples-the rate of wear increases, while resistance to wear decreases with an increase in load. Results showed that the friction coefficient and wear rate were highly influenced by load [31]. In Fig. 11 the variation of wear rate with respect to COF and load has been plotted. Fig. 12 and Fig. 13 depict the surface plot (wireframe) and contour plot of wear rate with respect to COF and load for the sample sintered at 450^{0}C respectively.

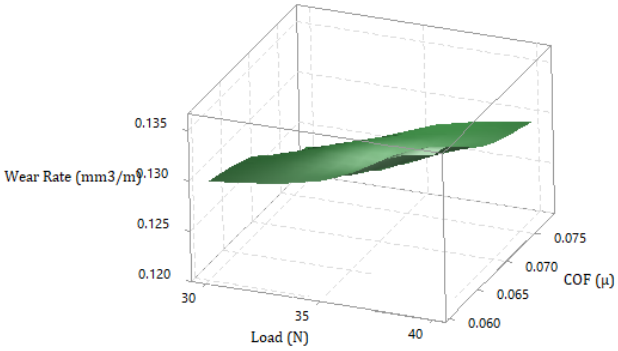

Fig. 11. Surface Plot of Wear Rate vs COF and Load for the sample sintered at 450^{0}C.

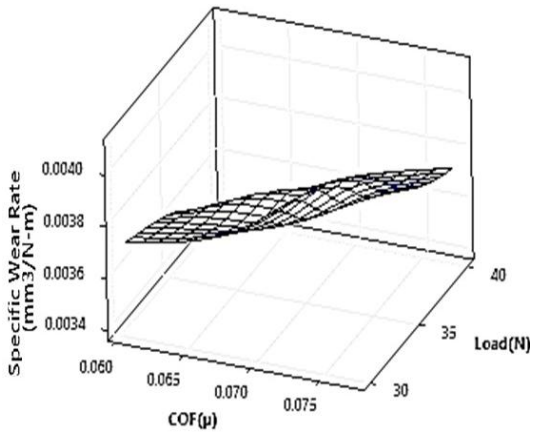

Fig.12. Surface Plot (Wire-frame) of Specific Wear Rate vs CoF and Load for the sample sintered at 450^{0}C.

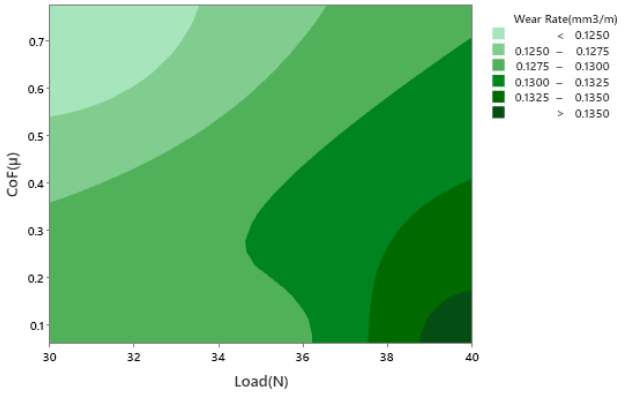

Fig. 13. Contour Plot of Wear Rate vs CoF and Load for the sample sintered at 450^{0}C.

A decrease in the coefficient of friction implies the material becomes less resistant to sliding motion at higher loads. This could be due to factors like increased contact area, a rise in temperature, or changes in the lubrication regime.

Wear rate increases as higher loads generally lead to increased wear. The material is subjected to greater stress, which can accelerate wear mechanisms like abrasion, adhesive wear, and fatigue.

An increase in specific wear rate, often caused by changes in wear mechanisms or oxide layer formation, indicates a decrease in wear resistance, making the material more susceptible to wear at higher loads.

Apart from it aspects like material properties and operating conditions such as lubrication, surface finish, humidity, temperature, presence of contaminants etc., can impact wear. The results demonstrated that increased applied load and sintering temperature result in higher wear rates and lower wear resistance. Supporting data, including a time vs wear plot and friction graph, are provided (Fig. 14) for a sample sintered at 450^{0}C.

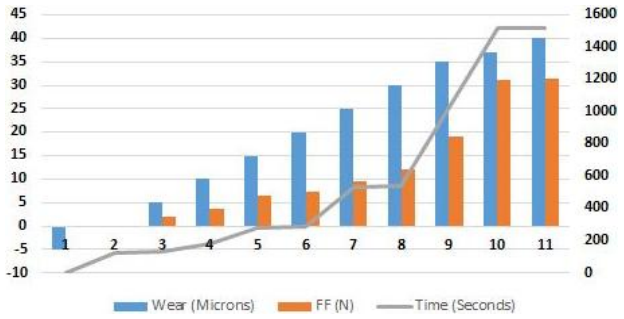

Fig. 14. Wear and friction vs. time plot for the sintered (450^{0}C) sample.

After conducting the wear test on the said sample (sintered at 450^{0}C) at 40 N load conditions, FESEM images (Fig. 15) as well as (Fig. 16) were analysed.

The wear pattern of the sample was examined through imaging, and the FESEM image reveals evidence of abrasive wear, characterized by plough marks that follow the sliding direction.

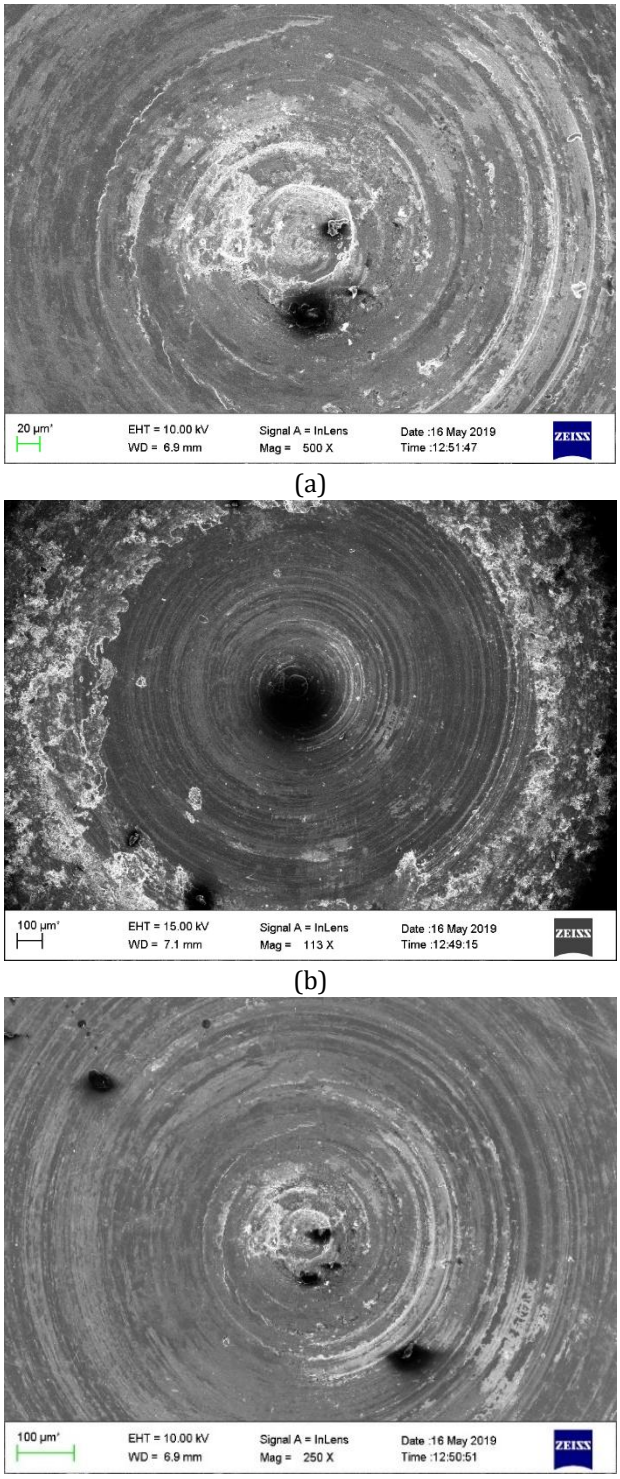

Fig. 15. (a), (b), (c) FESEM images of the worn-out sample sintered at 450°C.

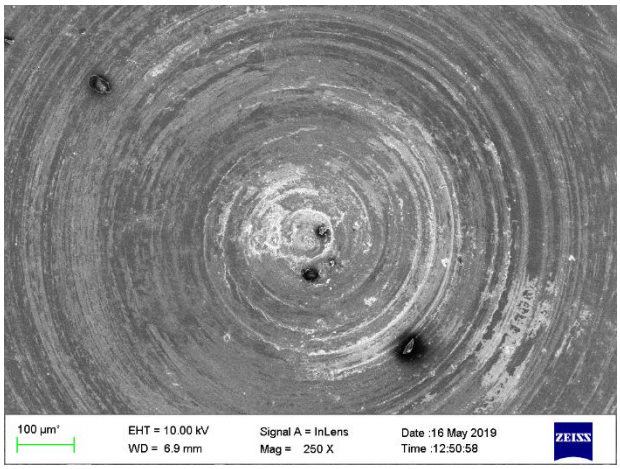

(a)

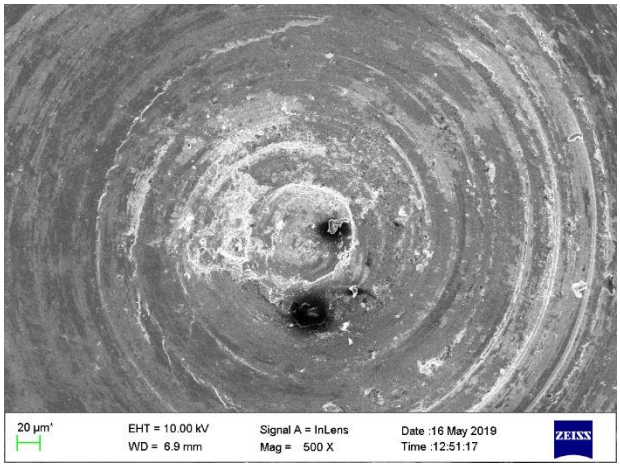

(b)

Fig. 16. (a), (b) Detailed FESEM images of worn sample surface after wear test.

4.3 Analysis of coefficient of friction

Table 7. Two-way ANOVA against COF.

Source of Variation	DF	SS	MS	F	p-Value
Speed	3	0.18	0.06	3	0.0471
Load	3	0.2	0.067	3.33	0.0345
Percentage of Al_2O_3 (PA)	1	0.2	0.2	1	0.3263
Speed*Load	9	0.12	0.013	0.67	0.7432
Speed*PA	3	0.01	0.003	0.17	0.9183
Load*PA	3	0.01	0.003	0.17	0.9183
Error	16	0.32	0.02	-	-
Total	38	1.04	-	-	-

DF - Degree of Freedom; **SS**: Sum of Squares due to the source; **MS**: Mean of Squares due to the source; **F value**: ratio of the mean square of the independent variable to the mean square of the residuals; **p-Value**: probability of getting the observed F value, (The p-values indicate the probability of observing the test results under the null hypothesis).

Main effects -The two-way ANOVA table (Table 7) indicates that both speed and load have a significant effect on the coefficient of friction ($p = 0.0471$ and $p = 0.0345$, respectively). This suggests that changes in speed and load result in statistically significant changes in coefficient of friction and that the percentage of alumina (PA) does not contribute to the variation in coefficient of friction.

Speed -The F-statistic for speed is 3.00, which indicates that the variation in coefficient of friction due to speed is three times larger than the variation due to random error. The p-value of 0.0471 indicates that the probability of observing this result by chance is less than 5%. Therefore, we can conclude that speed has a statistically significant effect on the coefficient of friction.

Load - The F-statistic for Load is 3.33, which indicates that the variation in the response variable due to Load is 3.33 times larger than the variation due to random error. The p-value of 0.0345 indicates that the probability of observing this result by chance is less than 5%. Therefore, we can conclude that Load has a statistically significant effect on the response variable.

Interaction effects - The two-way ANOVA table also indicates that there are no significant interactions between speed and load, speed and PA, or load and PA. This suggests that the effects of speed and load on the coefficient of friction do not depend on the level of the other factor.

PA - The F-statistic for PA is 1.00, which indicates that the variation in the coefficient of friction due to PA is equal to the variation due to random error. The p-value of 0.3263 indicates that the probability of observing this result by chance is greater than 5%. Therefore, we can conclude that PA does not have a statistically significant effect on the coefficient of friction.

Error - The error term in the ANOVA table represents the variation in the response variable that cannot be explained by the factors. The mean square error (MSE) is 0.02, which indicates that the average variation in the coefficient of friction due to random error is 0.02.

4.4 Tribological analysis (input parameters and performance characteristics)

In this tribological analysis, rate of wear, specific wear rate, relative resistance to wear and the frictional coefficient values with different parameter settings have been listed in Table-5 and Table-6. The GRA method was successfully used to optimize the wear characteristics of the Al/Al_2O_3 functionally graded composite material, and subsequent ANOVA analysis revealed the most critical parameters influencing wear behaviour and confirmed the accuracy of the model [32-33].

4.5 Grey relational analysis

The values for wear rate, specific wear rate, relative wear resistance, and coefficient of friction values have been recorded for further evaluation in tables 5 and 6, respectively. GRA, as described in section 2.3, was carried out using the above data. The process output characteristics were normalized (Ref. Table 9) with the smaller the better approach using Eq.-2.

Further using Eq.-5, the grey relational coefficient was calculated and the corresponding GRG and rank values were listed in Table-11. GRG for Experiment-1 was calculated to be 0.811, which showed optimal parameter setting to obtain the optimum result among all the experiments conducted.

With the aid of Minitab software, a response table from the GRG data and input process parameters was generated. The "higher-the-better" methodology was subsequently applied to identify the optimal values for each input parameter. A rank of the settings was calculated based on the value of Δ (Δ was the difference between maximum and minimum input values). Thus, in the tribological analysis of the new FGCM developed using Aluminium and Alumina, speed was the most influential factor (as indicated in the ranking), followed by load.
Based on the process output with reference to corresponding parametric conditions obtained from the experiment (Table 8), the optimal process parameters should be 300 m/s speed with 30 N loads, respectively.
According to the response plots (Figs. 8-13), reducing speed and load leads to improved grey relational grades. Although all inputs yield grades above 0.8, speed is identified as the most critical parameter in minimizing wear rate.

Table 8. Process output with reference to the corresponding parametric conditions.

Expt. No.	Speed	Load	Time	Dia	WR	SWR	RWR	CoF
1	300	30	30	5	0.1203	0.004	8.313	0.071
2	300	35	30	5	0.1234	0.0035	8.105	0.067
3	300	40	30	5	0.1265	0.0032	7.908	0.060
4	300	45	30	5	0.1293	0.0028	7.740	0.051
5	350	30	30	5	0.1232	0.0038	8.323	0.065
6	350	35	30	5	0.1254	0.0033	8.131	0.062
7	350	40	30	5	0,1272	0.0032	7.943	0.055
8	350	45	30	5	0.1304	0.0028	7.755	0.048
9	400	30	30	5	0.1273	0.0038	8.331	0.062
10	400	35	30	5	0.1288	0.0035	8.139	0.056
11	400	40	30	5	0.1293	0.0033	7.956	0.053
12	400	45	30	5	0.1328	0.0029	7.773	0.050
13	450	30	30	5	0.1308	0.0039	8.342	0.057
14	450	35	30	5	0.1306	0.0035	8.151	0.054
15	450	40	30	5	0.1318	0.0033	7.974	0.051
16	450	45	30	5	0.1361	0.0029	7.797	0.048
			Max	0	0.1361	0.004	8.342	0.071
			Min	0	0.1203	0.0028	7.740	0.048

The results of 16 experiments investigating the effects of speed, load, and time on wear rate, specific wear rate, relative wear resistance, and CoF have been demonstrated in Table 8.

The experiments were carried out at distinct speeds (300, 350, 400, and 450 RPM), loads (30, 35, 40, and 45 Newton), and times (30 minutes).

Crucial outcomes

- Wear rate and specific wear rate increase with increasing load and speed.
- Relative wear resistance decreases with increasing factors i.e., load and speed.
- CoF decreases with increasing value of factor load and speed.
- The highest wear rate (0.13605 m^3/m) and lowest coefficient of friction (0.0483) were observed at the highest speed (450) and load (45).
- The lowest wear rate (0.1203m^3/m) and highest coefficient of friction (0.0707) were observed at the lowest speed (300) and load (30). The results suggest that increasing speed and load lead to increased wear and decreased wear resistance, while also affecting the coefficient of friction. These findings can help in the design and optimization of the tribological systems.

The data in Table 9 has been normalized to a scale of 0 to 1, representing the minimum and maximum values, respectively, for wear rate, specific wear rate, relative wear resistance, and COF.

Table. 9. Normalized performance characteristic values.

	WR	SWR	RWR	COF
	1	**0**	0.952	**1**
	0.803	0.4	0.607	0.84
	0.606	0.64	0.278	0.51
	0.429	0.96	**0**	0.11
	0.819	0.2	0.968	0.73
	0.676	0.52	0.649	0.59
	0.565	0.68	0.336	0.29
	0.359	**1**	0.024	**0**
	0.556	0.16	0.982	0.61
	0.46	0.44	0.663	0.33
	0.429	0.6	0.359	0.19
	0.206	0.92	0.055	0.06
	0.333	0.12	**1**	0.37
	0.349	0.4	0.682	0.25
	0.27	0.56	0.388	0.13
	0	0.88	0.094	0.01
Max	1	1	1	1
Min	0	0	0	0

Note: CoF: Coefficient of Friction; WR: Wear Rate (m^3/m); SWR: Specific Wear Rate (mm^3/N-m); RWR: Relative Wear Resistance (per kg or per m^3)

Crucial outcomes

- Wear rate and specific wear rate exhibit similar distribution patterns, with values spanning from 0 to 1.
- In contrast, relative wear resistance shows greater variability, ranging from 0.11 to 1, while COF displays less variability, with values between 0.01 and 0.96.
- The normalized results allowed for a comparison of the different parameters on the same scale. The wear rate and specific wear rate showed similar distributions, while the relative wear resistance and COF showed distributions that were more distinct.
- This could help identify patterns and correlations between the parameters.

Table 10 here presented the deviation sequence of wear rate, specific wear rate, relative wear resistance, and coefficient of friction (COF). The values represented the difference between each data point and the minimum value.

Table 10. Deviation sequence of performance characteristic values.

	WR	SWR	RWR	COF
	0	**1**	0.048	**0**
	0.197	0.6	0.393	0.16
	0.394	0.36	0.722	0.486
	0.571	0.04	**1**	0.895
	0.181	0.8	0.032	0.267
	0.324	0.48	0.351	0.412
	0.435	0.32	0.664	0.706
	0.641	**0**	0.976	**1**
	0.444	0.84	0.018	0.392
	0.54	0.56	0.337	0.675
	0.571	0.4	0.641	0.808
	0.794	0.08	0.945	0.942
	0.667	0.88	**0**	0.626
	0.651	0.6	0.318	0.748
	0.73	0.44	0.612	0.871
	1	0.12	0.906	0.993
Max	1	1	1	1
Min	0	0	0	0

Crucial outcomes

- Wear rate and specific wear rate seem to have similar deviation sequences, with a maximum and minimum deviation of 1 and 0 respectively.
- Relative wear resistance had a more varied deviation sequence, with a maximum deviation of 1 and a minimum deviation of 0.018.
- COF had a relatively consistent deviation sequence, with a maximum deviation of 0.993 and a minimum deviation of 0.04.
- The deviation sequence analysis highlights the spread of each parameter from its minimum value.
- The wear rate and specific wear rate have similar spreads, while the relative wear resistance and COF had more distinct spreads.

This can help identify patterns and correlations between the parameters.

Table 11. Grey relational coefficient with corresponding rank.

WR	SWR	RWR	COF	GRG	Rank
1	0.333	0.912	1	0.81	1
0.718	0.455	0.56	0.76	0.62	3
0.56	0.581	0.409	0.51	0.51	9
0.467	0.926	0.333	0.36	0.52	8
0.734	0.385	0.941	0.65	0.68	2
0.607	0.51	0.587	0.55	0.56	5
0.535	0.61	0.43	0.42	0.5	10
0.438	1	0.339	0.33	0.53	7
0.529	0.373	0.965	0.56	0.61	4
0.481	0.472	0.597	0.43	0.49	11
0.467	0.556	0.438	0.38	0.46	14
0.387	0.862	0.346	0.35	0.49	12
0.429	0.362	1	0.44	0.56	6
0.434	0.455	0.611	0.4	0.48	13
0.406	0.532	0.45	0.37	0.44	16
0.333	0.806	0.356	0.34	0.46	15

Wear rate and specific wear rate

- The wear rate (m^3/m) and specific wear rate ($mm^3/N\text{-}m$) values vary across the samples, indicating differences in wear resistance.
- Samples 1, 10, and 12 exhibit relatively low wear rates and high specific wear rates, suggesting better wear resistance.

Relative wear resistance

- The relative wear resistance values (/kg or $/m^3$) show a range of performance, with Samples 1, 10, and 12 ranking high.
- This suggests that these samples have improved wear resistance compared to others.
- COF (Coefficient of Friction):
- COF values range from 0.33 to 0.81, indicating varying frictional properties.
- Lower COF values typically indicate reduced friction and wear.

GRG (Grey relational grade)

- GRG values range from 0.455 to 1, indicating differences in surface gloss and smoothness.
- Higher GRG values typically indicate better surface finish.

Rank

- The rank column suggests an overall performance ranking, with Sample 1 ranking highest.
- This ranking considers a combination of wear rate, specific wear rate, relative wear resistance, COF, and GRG.

Trends and observations

- Samples with lower wear rates and higher specific wear rates tend to have better relative wear resistance and lower COF values.
- Improved surface finish (higher GRG) may contribute to better wear resistance and reduced friction.

5. CONCLUSIONS

Al/Al_2O_3 FGCM samples with a density ranging more than 90% were fabricated using uniaxial hot press at varied sintering temperatures with desired layers and compositions. It was observed that the layers in the sintered sample were well stacked and discrete, confirming uniform gradation. Hardness was measured at each individual layer of each sample, and it showed different values, and it showed a

gradual increase corresponding to the increase in Al_2O_3 reinforcement. For a 40N applied load, the FGCM samples (sintered at 400^0C and 450^0C respectively) exhibited wear rates of 0.1265 & 0.1357 mm^3/m respectively, which implied wear rate increased with the rise in sintering temperatures. The effects of load, sliding speed, and alumina weight percentage on the dry sliding wear of aluminum-based FGCMs were investigated using the Taguchi method.

Key findings of the study have been summarized underneath:

a. The wear rate was primarily influenced by load and sliding speed, with increasing load leading to a substantial rise in wear rate, while higher sliding speeds resulted in a moderate decrease. The results showed that load had a significant impact on wear rate, with increased load leading to increased wear. In contrast, sliding speed had a moderate effect: with higher speeds, the wear rate reduced.

b. The study found that the coefficient of friction was strongly affected by load, sliding speed, and alumina content. Specifically, increased load led to a significant rise in friction coefficient, while higher sliding speeds resulted in a moderate decrease.

c. The findings indicated that wear rate and friction coefficient were influenced by load and sliding speed. Increased load led to higher wear rates and friction coefficients, whereas higher sliding speeds had the opposite effect. Thus, it may be concluded that load and sliding speed were critical factors influencing wear rate and friction coefficient. Increased load resulted in increased wear and friction, while higher sliding speeds led to decreased wear and friction.

Acknowledgement:

The authors are highly obliged to SOA University and Dr. A.K. Chaubey, CSIR-IMMT, for the guidance, support, and help in conducting the experiments and carrying out the research work at different stages of the work.

REFERENCES

[1] M. Yamanouchi, M. Koizumi, T. Hirai, and I. Shiota, *Proceedings of the 1st International Symposium on Functionally Gradient Materials*, Sendai, Japan, Oct. 8–9, 1990.

[2] D. K. Jha, T. Kant, and R. K. Singh, "A critical review of recent research on functionally graded plates," *Composite Structures*, vol. 96, pp. 833–849, Sep. 2012, doi: 10.1016/j.compstruct.2012.09.001.

[3] A. Tripathy, S. K. Sarangi, A. K. Chaubey, and U. K. Mohanty, "Fabrication of AL/AL2O3 functionally graded material using powder metallurgy route," in *Learning and analytics in intelligent systems*, 2019, pp. 377–387. doi: 10.1007/978-3-030-30271-9_35.

[4] A. Tripathy, A. K. Chaubey, and S. K. Sarangi, "A case study on AL/AL2O3 ultrafine composites fabricated using PM Route," in *Learning and analytics in intelligent systems*, 2019, pp. 260–269. doi: 10.1007/978-3-030-30271-9_24.

[5] A. Pasha and B. M. Rajaprakash, "Fabrication and mechanical properties of functionally graded materials: A review," *Materials Today Proceedings*, vol. 52, pp. 379–387, Sep. 2021, doi: 10.1016/j.matpr.2021.09.066.

[6] A. Tripathy, R. Gupta, S. K. Sarangi, and A. K. Chaubey, "Design and fabrication of Aluminium/Alumina ultra-fine composite and functionally graded material using powder metallurgy route," in *Lecture notes on multidisciplinary industrial engineering*, 2019, pp. 739–747. doi: 10.1007/978-981-32-9471-4_62.

[7] R. F. Silva *et al.*, "Functionally graded materials and structures: unified approach by optimal design, metal additive manufacturing, and Image-Based Characterization," *Materials*, vol. 17, no. 18, p. 4545, Sep. 2024, doi: 10.3390/ma17184545.

[8] A. Tripathy, S. K. Sarangi, and A. K. Chaubey, "A review of solid state processes in manufacture of functionally graded materials," *International Journal of Engineering & Technology*, vol. 7, no. 4.39, pp. 1–5, Dec. 2018, doi: 10.14419/ijet.v7i4.39.23686.

[9] V. Bhavar, P. Kattire, S. Thakare, S. Patil, and R. Singh, "A review on Functionally Gradient Materials (FGMs) and their applications," *IOP Conference Series Materials Science and Engineering*, vol. 229, p. 012021, Sep. 2017, doi: 10.1088/1757-899x/229/1/012021.

[10] A. Tripathy, S.K. Sarangi and R.K. Panda, "Fabrication of functionally graded composite material using powder metallurgy route: an overview," *International Journal of Mechanical and Production Engineering Research and Development (IJMPERD)*, vol. 7, no. 6, pp. 135-146, Dec. 2017.

[11] I. M. El-Galy, B. I. Saleh, and M. H. Ahmed, "Functionally graded materials classifications and development trends from industrial point of view," *SN Applied Sciences*, vol. 1, no. 11, Oct. 2019, doi: 10.1007/s42452-019-1413-4.

[12] M. Naebe and K. Shirvanimoghaddam, "Functionally graded materials: A review of fabrication and properties," *Applied Materials Today*, vol. 5, pp. 223–245, Oct. 2016, doi: 10.1016/j.apmt.2016.10.001.

[13] J. Sheraf and D. G. S, "Synthesis and characterization of 4-layered Functionally graded Al-Al2O3 MMC," *Heliyon*, vol. 10, no. 20, p. e39289, Oct. 2024, doi: 10.1016/j.heliyon.2024.e39289.

[14] Y. H. Fei, C. Z. Huang, H. L. Liu, and B. Zou, "Mechanical properties of Al2O3–TiC–TiN ceramic tool materials," *Ceramics International*, vol. 40, no. 7, pp. 10205–10209, Mar. 2014, doi: 10.1016/j.ceramint.2014.03.056..

[15] M. J. Ghazali, W. M. Rainforth, and H. Jones, "Dry sliding wear behaviour of some wrought, rapidly solidified powder metallurgy aluminium alloys," *Wear*, vol. 259, no. 1–6, pp. 490–500, May 2005, doi: 10.1016/j.wear.2005.02.089.

[16] F.P. Bowden, and D. Tabor, *The Friction and Lubrication of Solids*, Clarendon Press, Oxford, 1986.

[17] J. Singh and A. Chauhan, "Overview of wear performance of aluminium matrix composites reinforced with ceramic materials under the influence of controllable variables," *Ceramics International*, vol. 42, no. 1, pp. 56–81, Sep. 2015, doi: 10.1016/j.ceramint.2015.08.150.

[18] B. Heer, Y. Zhang, and A. Bandyopadhyay, "Additive manufacturing of alumina-silica reinforced Ti6Al4V for articulating surfaces of load-bearing implants," *Ceramics International*, vol. 47, no. 13, pp. 18875–18885, Mar. 2021, doi: 10.1016/j.ceramint.2021.03.227.

[19] S. Ahmad *et al.*, "Experimental studies on mechanical properties of Al-7075/TiO2 metal matrix composite and its tribological behaviour," *Journal of Materials Research and Technology*, vol. 30, pp. 8539–8552, May 2024, doi: 10.1016/j.jmrt.2024.05.227.

[20] Z. J. Wang, Z. Zheng, and M. W. Fu, "Aluminum matrix composites: Structural design and microstructure evolution in the deformation process," *Journal of Materials Research and Technology*, vol. 30, pp. 3724–3754, Apr. 2024, doi: 10.1016/j.jmrt.2024.03.237.

[21] R. K. Verma, D. Parganiha, and M. Chopkar, "A review on fabrication and characteristics of functionally graded aluminum matrix composites fabricated by centrifugal casting method," *SN Applied Sciences*, vol. 3, no. 2, Jan. 2021, doi: 10.1007/s42452-021-04200-8.

[22] M. Tayyebi and M. Alizadeh, "Thermal and wear properties of Al/Cu functionally graded metal matrix composite produced by severe plastic deformation method," *Journal of Manufacturing Processes*, vol. 85, pp. 515–526, Dec. 2022, doi: 10.1016/j.jmapro.2022.11.059.

[23] O. P. Modi, R. P. Yadav, D. P. Mondal, R. Dasgupta, S. Das and A. H. Yegneswaran, "Abrasive Wear Behaviour of Zinc Aluminium Alloy 10% Alumina Composite Through Factorial Design of Experiment", *Journal of Materials Science*, vol. 36, pp. 1601-1607, Apr. 2001, doi: 10.1023/A:1017523214073.

[24] Y. Sahin, "The prediction of wear resistance model for the metal matrix composites," *Wear*, vol. 258, no. 11–12, pp. 1717–1722, Apr. 2005, doi: 10.1016/j.wear.2004.11.024.

[25] E. Rabinowicz, *Friction and Wear of Materials, 2nd Edition*, John Wiley & Sons Inc., New York, 2013.

[26] S. Wilson and A. T. Alpas, "Wear mechanism maps for metal matrix composites," *Wear*, vol. 212, no. 1, pp. 41–49, Nov. 1997, doi: 10.1016/s0043-1648(97)00142-7.

[27] A. M. Al-Qutub, I. M. Allam, and M. a. A. Samad, "Wear and friction of Al–Al2O3 composites at various sliding speeds," *Journal of Materials Science*, vol. 43, no. 17, pp. 5797–5803, Aug. 2008, doi: 10.1007/s10853-008-2867-8.

[28] T. Barik, S. K. Jena, S. Gahir, K. Pal, and S. K. Pattnaik, "Process parametric optimization in drilling of CFRP composites using GRA method," *Materials Today Proceedings*, vol. 39, pp. 1281–1286, May 2020, doi: 10.1016/j.matpr.2020.04.220.

[29] T. S. Kumar, R. Raghu, and S. Shalini, "Hardness and wear behavior of AL 6061/ZRC composite processed by friction stir processing," *Tribology in Industry*, vol. 42, no. 4, pp. 582–591, Dec. 2020, doi: 10.24874/ti.855.02.20.10.

[30] S. Basavarajappa, G. Chandramohan, and J. P. Davim, "Application of Taguchi techniques to study dry sliding wear behaviour of metal matrix composites," *Materials & Design (1980-2015)*, vol. 28, no. 4, pp. 1393–1398, Mar. 2006, doi: 10.1016/j.matdes.2006.01.006.

[31] S. Dharmalingam, R. Subramanian, and K. S. Vinoth, "Analysis of Dry Sliding Friction and Wear Behavior of Aluminum-Alumina Composites using Taguchi's Techniques," *Journal of Composite Materials*, vol. 44, no. 18, pp. 2161–2177, Mar. 2010, doi: 10.1177/0021998310365175.

[32] M.S. Surya, G. Prasanthi, "Tribological behaviour of aluminum silicon carbide functionally graded material," *Tribology in Industry*, vol. 40, no. 2, pp. 247–253, Jun. 2018, doi: 10.24874/ti.2018.40.02.08.

[33] J. Ross Phillip, *Taguchi Technique for Quality Engineering*, McGraw-Hill, New York, 1988.